Hindawi
Advances in Meteorology
Volume 2017, Article ID 6124149, 17 pages
https://doi.org/10.1155/2017/6124149

Research Article

Attenuation Correction of Weather Radar Reflectivity with Arbitrary Oriented Microwave Link

Peng Zhang,[1,2] Xichuan Liu,[2] Zhaoming Li,[3] Zeming Zhou,[2] Kun Song,[2] and Pinglv Yang[2]

[1]*Army Engineering University of PLA, Nanjing 210007, China*
[2]*College of Meteorology and Oceanology, National University of Defense Technology, Nanjing 211101, China*
[3]*LAGEO, Institute of Atmospheric Physics, UCAS, Beijing 100029, China*

Correspondence should be addressed to Peng Zhang; zhangpeng_meteo@yahoo.com

Received 17 July 2017; Revised 20 November 2017; Accepted 7 December 2017; Published 31 December 2017

Academic Editor: Youcun Qi

To compensate radar reflectivity for attenuation effect, a new method for attenuation correction of the radar reflectivity using arbitrary oriented microwave link (referred henceforth to as ACML) is developed and evaluated. Referring to the measurement of arbitrary oriented microwave link, the ACML method optimizes the ratio of specific attenuation to specific differential phase which is a key parameter in attenuation correction schemes. The proposed method was evaluated using real data of a dual-polarization X-band radar and measurements of two microwave links during two rainstorm events. The results showed that the variation range of the optimized ratio was overall consistent with the results of the previous studies. After attenuation correction with the optimal ratios, the radar reflectivity was significantly compensated, especially at long distances. The corrected reflectivity was more intense than the reflectivity corrected by the "self-consistent" (SC) method and closer to the reflectivity of a nearby S-band radar. The effectiveness of the method was also verified by comparing the rain rates estimated by the X-band radar with those derived by rain gauges. It is demonstrated that arbitrary oriented microwave link can be adopted to optimize the attenuation correction of radar reflectivity.

1. Introduction

Weather radar plays an important role in weather surveillance due to its high spatial-temporal resolution. Compared with the long wavelength (e.g., S- and C-band) radars, short wavelength (e.g., X-band) radars have some advantages, including smaller-sized antenna and higher sensitivity of the differential phase shift to rain rate. An urban remote sensing network composed of eight dual-polarization (DP) X-band radars was deployed to overcome the WSR-88DP coverage limitations and provide flash flood warnings [1]. However, the impact of attenuation caused by precipitation at higher frequencies needs to be compensated for successful implementation of quantitative precipitation estimation (QPE). Various methods have been developed to correct the attenuated radar reflectivity. However, because the actual amount of attenuation is unknown, the existing methods for attenuation correction still have many problems. Hitschfeld and Bordan (1954) demonstrated that their HB algorithm is inherently unstable and certain constraints imposing on the total attenuation are required [2]. For dual-polarized radar, many attenuation correction algorithms were developed. They are based on the property that the differential propagation phase φ_{DP} is nearly linearly proportional to cumulative attenuation in typical radar frequencies [3]. Testud et al. (2000) proposed a correction algorithm (the ZPHI rain profiling algorithm), which assumed a fixed proportionality constant of the dependence of specific attenuation A_H on specific differential phase K_{DP} [4]. But the ZPHI algorithm is very sensitive to the proportionality constant. To tackle this problem, many studies have focused on the determination of the correction coefficients. Bringi et al. (2001) proposed the so-called "self-consistent" method (SC), in which an optimal proportionality constant of A_H/K_{DP} is estimated by comparing the calculated φ_{DP} with the measured φ_{DP} [5]. Based on SC method, Park et al. (2005) modified the attenuation correction method for the X-band frequency [6]. To track

variability in drop size distribution (DSD), Lim and Chandrasekar (2006) developed a dual-polarization rain profiling algorithm (DRPA) incorporating reflectivity as well as differential reflectivity profiles with attenuation. A self-consistent method corresponding to the DRPA (SC-DRPA) was also proposed to get the optimal correction coefficients [7]. The DRPA method has been improved through being less affected by the bias of reflectivity and differential reflectivity [8]. Rico-Ramirez (2012) extended HB and Iguchi's "Final Value" (FV) [9] algorithms to make the correction coefficients adaptive by parameter optimization in a similar way to the SC method [10]. Kalogiros et al. (2014) provided the self-consistent with optimal parameterization (SCOP) algorithm for attenuation correction of radar reflectivity which uses optimal parameterization and best-fitted functions of specific attenuation and backscattering differential phase shift [11]. It can be seen from these studies that the coefficient optimization is critical for improving the effectiveness of the proposed methods.

Recently, a variety of investigations have focused on using existing microwave links which widely spread across countries for rain monitoring, validating, and optimizing the radar-based QPE, attenuation correction of radar observations, and so forth [e.g., [12, 13]]. It is concluded that path averaged precipitation estimated by the attenuation along the link path is more compatible with radar observations than point measurements by gauges [14]. Krämer et al. (2005) adopted the attenuation and rainfall information derived from a microwave link with its receiver colocated with an X-band weather radar as a reference to correct the radar data for rainfall estimation [15]. Using the same link as in [15], Rahimi et al. (2006) presented a backward-iterative attenuation correction algorithm on which the link attenuation constraint was imposed [16]. Trömel et al. (2014) demonstrated that the ratio of A_H/K_{DP} can be optimized with the help of microwave links oriented along radar radial [14]. However, in these studies focusing on attenuation correction of radar observations using microwave link measurements, the utilized links are required to be along the radar radial direction. This restrains the applications of arbitrary oriented microwave links and those proposed algorithms. In addition, because only the radar observations of the ray along which the microwave link is located can be corrected, the effectiveness of those methods is also reduced.

To tackle these problems, this paper proposes a method for attenuation correction of radar reflectivity by using measurement of arbitrary oriented microwave link. The proposed method was evaluated with real data of a dual-polarization X-band radar and the records of two microwave links during two rainstorm events. The validity of the method was demonstrated by comparing the corrected reflectivity with the result of the SC method and with the reflectivity of a nearby S-band weather radar. The effectiveness was also evaluated by comparing the rain rates estimated by the X-band radar with those derived by rain gauges. The results show that the ACML provides an alternative approach to optimize the correction coefficients and broaden the application scope of microwave links in attenuation correction of radar reflectivity and QPE. This paper is organized as follows. The proposed ACML algorithm is described in Section 2. Section 3 presents the experiments and the important results. Finally, the conclusions are presented in Section 4.

2. Methodology

The ACML is based on the ZPHI rain profiling method [4]. Firstly, brief introduction of the ZPHI and the SC [5] algorithms is given.

2.1. The ZPHI and SC Algorithms. The specific attenuation $A_H(r)$ [in dB/km] and the measured reflectivity $Z'_H(r)$ [in $\mathrm{mm}^6/\mathrm{m}^3$] at range r can be expressed as

$$A_H(r) = a\left[Z_H(r)\right]^b, \tag{1}$$

$$Z'_H(r) = Z_H(r)\, e^{-0.46\int_0^r A_H(s)ds}, \tag{2}$$

where Z_H is the intrinsic reflectivity. The path-integrated attenuation can be expressed with respect to Z_H and Z'_H as

$$2\int_{r_0}^{r} A_H(s)\, ds = 10\log_{10}\left[Z_H(r)\right] - 10\log_{10}\left[Z'_H(r)\right], \tag{3}$$

where r_0 is the range corresponding to the first resolution volume with precipitation. In the ZPHI algorithm, A_H is determined with a constraint that the two-way path-integrated attenuation PIA_2 is proportional to the total span of the propagation differential phase φ_{DP}:

$$\mathrm{PIA}_2 = \alpha\left[\varphi_{\mathrm{DP}}(r_1) - \varphi_{\mathrm{DP}}(r_0)\right] = \alpha\Delta\varphi_{\mathrm{DP}}(r_0, r_1), \tag{4}$$

where r_1 denotes the ending range of the precipitation. With this constraint, a final form of A_H can be described as

$$A_H(r) = \frac{\left[Z'_H(r)\right]^b\left[10^{0.1\alpha b\Delta\varphi_{\mathrm{DP}}} - 1\right]}{I(r_0, r_1) + \left[10^{0.1\alpha b\Delta\varphi_{\mathrm{DP}}} - 1\right] I(r, r_1)}, \tag{5}$$

where

$$I(r_0, r_1) = 0.46b\int_{r_0}^{r_1}\left[Z'_H(s)\right]^b ds,$$
$$I(r, r_1) = 0.46b\int_{r}^{r_1}\left[Z'_H(s)\right]^b ds, \tag{6}$$

and $r_0 < r < r_1$. It should be noted that the calculation of the A_H using (5) needs setting a priori values for the exponent b and the coefficient α in (1) and (4), respectively. Given that A_H and Z_H are less sensitive to variations of temperature and drop shape than other polarimetric variables [e.g., [17, 18]], the exponent b has a relatively small dynamic value ranging from 0.76 to 0.84 at X-band [19]. On the other hand, the coefficient α varies widely with temperature and drop shape. According to the scattering simulations under various temperatures and drop shapes, the coefficient α varies from about 0.05 to 0.11 $\mathrm{dB}(^\circ)^{-1}$ at C-band [20] and from 0.139 to 0.335 $\mathrm{dB}(^\circ)^{-1}$ at X-band [6]. So, a fixed value of α may

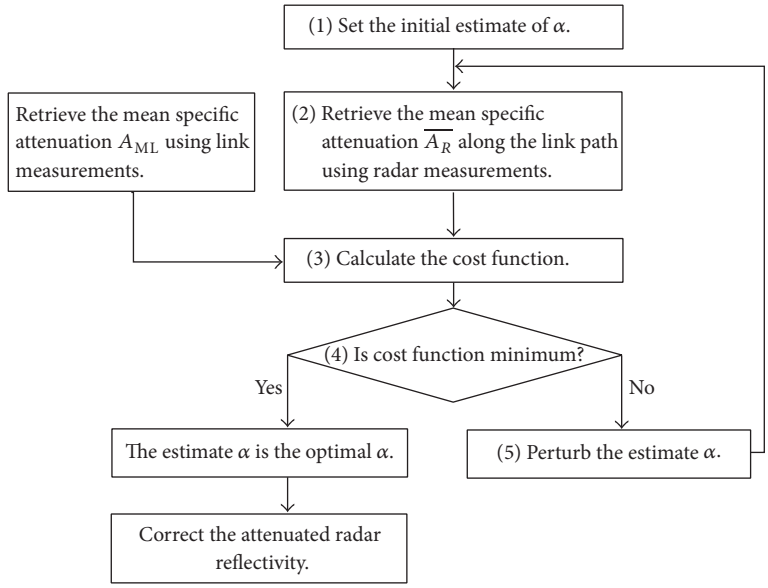

Figure 1: The flow schematic diagram of the optimization and correction algorithm.

introduce nonignorable errors in the retrieval of A_H, which in turn affects the attenuation correction of radar reflectivity. In SC method, an optimal α value is estimated based on self-consistent principle [5]. For a given α value, $A_H(r, \alpha)$ at each range is calculated by (5), and then $\varphi_{DP}^{cal}(r, \alpha)$ is given as

$$\varphi_{DP}^{cal}(r, \alpha) = 2 \int_{r1}^{r} \frac{A_H(s; \alpha)}{\alpha} ds. \quad (7)$$

The optimal α value is chosen when the difference between the calculated φ_{DP}^{cal} and the measured φ_{DP} over the entire range through an attenuating rain cell

$$\text{Error of } \varphi_{DP} = \sum_{i=1}^{N} \left| \varphi_{DP}^{cal}(r_i; \alpha) - \varphi_{DP}(r_i) \right| \quad (8)$$

is minimal, where i denotes the range gate index from r_0 to r_1 and N is the number of data points across the rain cell between r_0 and r_1.

2.2. The ACML Method. Instead of presetting a fixed α in ZPHI and estimating an optimal α from the radar data itself in SC, the ACML estimates the optimal α by an iterative process based on incorporating radar measurements and link measurements. In ACML, an initial value of α is set firstly and then the mean specific attenuations A_{ML} and $\overline{A}_R$ are retrieved with this α using link measurements and radar measurements, respectively. The optimal α is determined by minimizing the difference of A_{ML} and $\overline{A}_R$. The flow schematic diagram is shown in Figure 1.

2.2.1. Retrieval of Mean Specific Attenuation Using Microwave Link Measurements. Firstly, the attenuation baseline (or zero level) of microwave link should be determined to obtain the attenuation due to the rain along the link path. The baseline is not constant over time and fluctuates with changes of water vapor concentration, temperature, wind effects on the antenna, losses during transmission and reception, interferences, and possible multipath effects [21]. Therefore the calibration of the baseline (or zero level) is crucial for the link attenuation measurement [12]. Following the work of Chwala et al. (2012), the dry and wet (rainy) periods can be identified by considering the power spectrum of the received signal level (RSL) [22]. If the difference between powers in low frequency and high frequency regions exceeds a preset threshold, the period is identified as wet. In the ACML method, the radar can also be used as a wet/dry indicator. Furthermore, in our experiment, a rain gauge which was deployed just in the link path can be used as another wet/dry indicator. So, if the result of Chwala's method, or at least one radar pixel along the link, or the measurement of the rain gauge indicates that it is rainy, a wet period will be triggered. After identifying dry and wet periods, the baseline is set to the value just before a transition from a dry to a wet period. Then, the link attenuation due to precipitation Attenu_{ML} is obtained by subtracting the received power from the baseline. The mean specific attenuation A_{ML} (dB/km) can be retrieved based on microwave link as

$$A_{ML} = \frac{\text{Attenu}_{ML}}{L_{ML}}, \quad (9)$$

where L_{ML} (km) is the length of the link path. If the frequency of the link differs from that of the radar, it is necessary to transfer the attenuation at link frequency to that at radar frequency before comparing the mean specific attenuation retrieval results.

2.2.2. The Iterative Procedure. As shown in Figure 1, the iterative procedure to optimize the coefficient α is performed as follows. Firstly, the initial value of α is set to a certain

Table 1: Main characteristic values of the X-band radar and the S-band radar.

Radar	Transmitting frequency/GHz	Gate width/m	Antenna beam width/°	Range/km	Peak power/kw	Height of antenna/m
XR	9.19	75	1.5	60	75	15
SR	2.85	1000	0.99	460	650	138

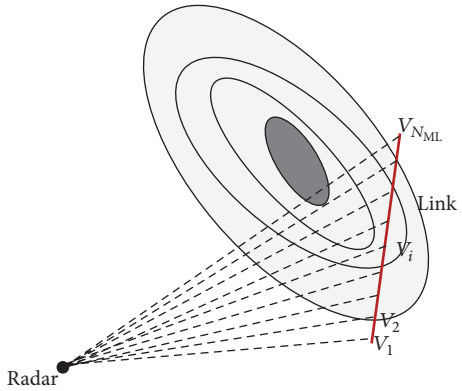

Figure 2: Sketch map of the retrieval of the mean specific attenuation along link path by radar.

range which can be determined from previous studies in the literatures (e.g., from 0.139 to 0.335 dB(°)$^{-1}$ in [6]).

Subsequently, with an estimate value of α along with (5), (6), and (10), the radar retrieved mean specific attenuation along link path $\overline{A_R}$ can be attained with

$$\overline{A_R} = \frac{\sum_{i=1}^{N_{ML}} A_{Hi}}{N_{ML}}, \tag{10}$$

where N_{ML} is the total number of radar measurement volumes along the link path (see Figure 2). It should be noted that since the distances from different parts of the link to radar are different, the volume size and height of each radar gate along link are different. Therefore, the specific attenuation is calculated in volumes of different sizes and heights. The difference of the radar measurement volume will increase with the distance from link to radar and will cause uncertainties in the estimation of $\overline{A_R}$. Moreover, when the link is far away from the radar, the radar and link will be more spatially mismatch. This will also cause uncertainties in the proposed method. So, to ensure the effectiveness of the method, the link cannot be too long.

Then a cost function (δA) which is defined as the difference between the mean specific attenuations retrieved by radar and link is calculated as

$$\delta A = \left| \overline{A_R} - A_{ML} \right|. \tag{11}$$

A golden-section search method [23] is applied here to find the optimal coefficient α that minimizes the cost function. In each iteration, given an interval $[\alpha_1, \alpha_2]$ which contains an extremum for cost function δA, the golden-section search method is performed by initially choosing two internal points α_3 and α_4 in the interval. The distance between the right-most internal point α_4 and the left-most endpoint α_1 equals to the distance between the right-most endpoint α_2 to the left-most internal point α_3. Both distances are equal to $0.618(\alpha_2 - \alpha_1)$. If $\delta A(\alpha_3) > \delta A(\alpha_4)$, the range of α for the next iteration will be set to $[\alpha_3, \alpha_2]$. Otherwise, the range will be set to $[\alpha_1, \alpha_4]$. Therefore, the range of α is narrowed by a fixed coefficient (0.618) after each iteration.

Finally, using the optimized value of α along with (5) and (6), the optimal specific attenuation $A_H(r; \alpha_{opt})$ at each gate of radar within the azimuth range which the link crosses can be retrieved, and the attenuated reflectivity can be corrected by (3).

3. Experiment and Results

To verify the effectiveness of the ACML method, data from two rainstorm cases were analyzed. For each case, data were obtained from an X-band dual-polarization radar (XR), an S-band single polarization radar (SR), a microwave link (ML), and six rain gauges. During these two cases, the radars (i.e., the XR and the SR) were the same, while the MLs and rain gauges were different. The MLs used in the two cases were different in transmitting frequency, range to radar, and link length. The effectiveness of the ACML method can be verified by comparing the corrected reflectivity with the reflectivity of the SR and the correction result of the SC method. The performance of the ACML method can also be evaluated by comparing the XR estimated rainfall with the gauge derived rainfall.

3.1. Data Sources. The locations of the XR, SR, two MLs, and twelve rain gauges used in experiments are indicated in Figure 3.

(a) Radars. Both the XR and the SR locate in Jiangsu province, China, and their main characteristic values are listed in Table 1.

The XR collected volume scan data with 2 or 4 elevations every 2 minutes. In each ray, it collected data from 800 gates of 75 m. The SR is located at 45.12 km southwest to the XR. It collected volume scan data with 11 elevations every 6 minutes. In each ray, it collected data from 460 gates of 1 km. Both radars were calibrated periodically.

(b) Microwave Links. To obtain the total path attenuation caused by the scattering and absorption of hydrometeors, the microwave link measures the transmitted energy between the transmitter and the receiver. The main parameter values of the MLs are listed in Table 2.

Both MLs transmitted and received horizontally polarized electric-magnetic wave without radomes. From the XR site, the transmitter of the ML1 was 46.12 km away and located

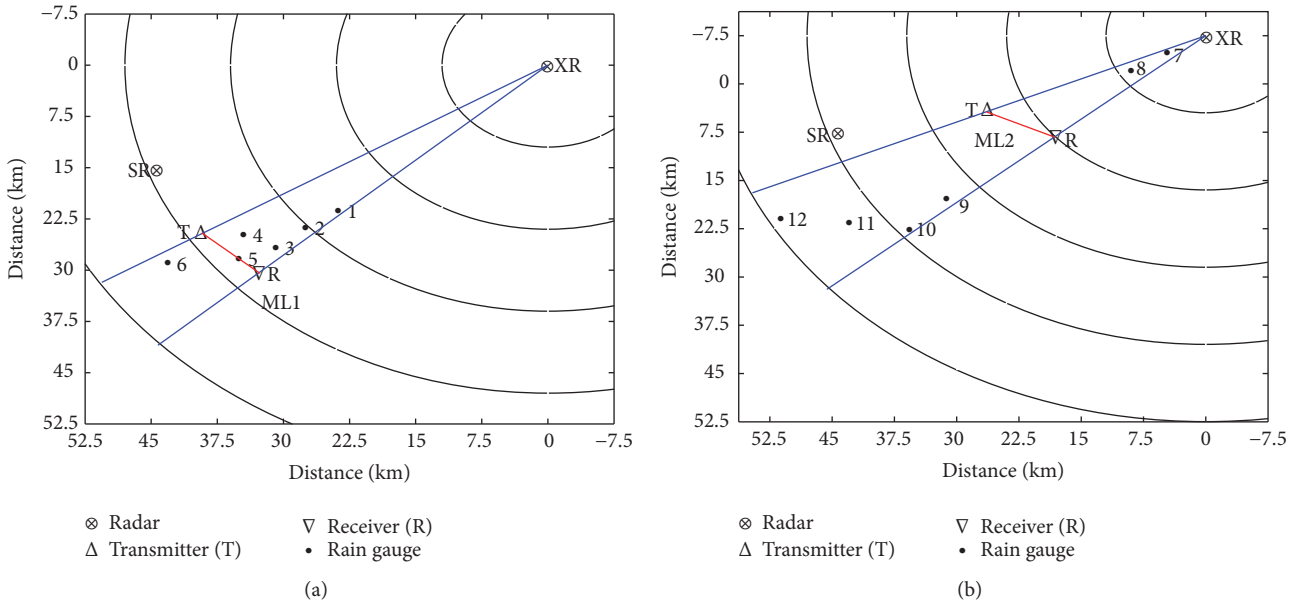

Figure 3: Diagram of the experiment area for (a) case I and (b) case II. The locations of the X-band radar, S-band radar, 2 microwave links, and 12 rain gauges are indicated. The circles correspond to X-band radar ranges of 12, 24, 36, 48, and 60 km, respectively.

Table 2: Main characteristic values of the microwave links.

ML	Frequency/GHz	Power/dBm	Length/km	Height of transmitter/m	Height of receiver/m	Beam width/°	Temporal resolution/s
ML1	9.47	20	7.5	76	112	7.5	15
ML2	7.7	24.5	8.66	126	152	3.5	60

at azimuth 237°, while the receiver was 44.62 km away and located at azimuth 228°. That is, the ML1 crossed 10° in azimuth (from 237° to 228°) of the XR. Compared with ML1, the ML2 was nearer to the XR. The transmitter of the ML2 was 29.13 km away and located at azimuth 245°, while the receiver of the ML2 was 24.05 km away and located at azimuth 230°. So, the ML2 crossed 16° in azimuth (from 245° to 230°) of the XR. The link attenuations were sampled by the two MLs with an accuracy of 0.01 dB. Note that the beam width of the ML1 was 7.5°, but it should be smaller to avoid the mismatching problem between radar beam and microwave link beam especially when the link path is long.

(c) Rain Gauges. As indicated in Figure 3, twelve tipping bucket rain gauges were deployed in the experiment area for the two cases. The sampling time interval of gauges 1 to 6 is 5 minutes and that of gauges 7 to 12 is 10 minutes. The resolution of all the gauges is 0.1 mm. The relative locations of the rain gauges to the XR are listed in Table 3. The distances from some gauges to the XR were longer than the link while some were shorter, which was helpful to evaluate the effectiveness of the proposed method. Note that gauge 5 was just in the path of ML1.

3.2. Analysis of Case I

3.2.1. Precipitation Event. A storm producing extreme heavy rainfall was observed by the experimental instruments on 2 June 2015. The precipitation was convective at first and then developed to a mixed type precipitation. A reflectivity field example measured by the XR is shown in Figure 4.

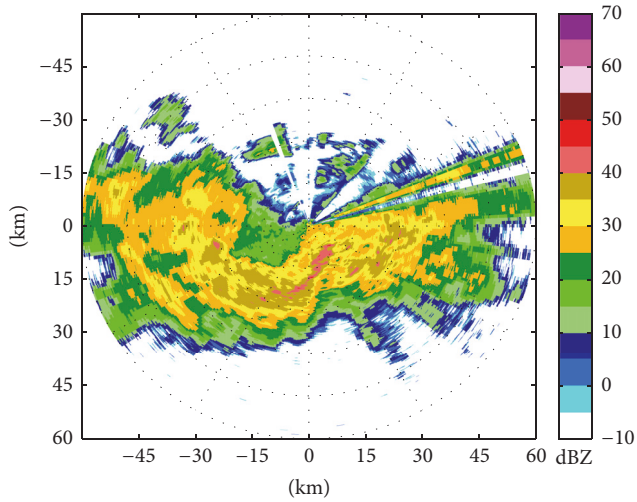

Figure 4: Reflectivity PPI at elevation 1° of the X-band radar at 0746 UTC, 2 June 2015. The circles correspond to radar ranges of 12, 24, 36, 48, and 60 km, respectively.

As seen from Figure 4, several convective cores immersed within stratiform precipitation echoes which indicated that

Table 3: Relative locations of the gauges to the radar.

	Gauge 1	Gauge 2	Gauge 3	Gauge 4	Gauge 5	Gauge 6	Gauge 7	Gauge 8	Gauge 9	Gauge 10	Gauge 11	Gauge 12
Azimuth/°	228	229	229	234	231	236	242	240	232	230	235	241
Distance/km	31.95	36.38	40.86	42.30	45.01	51.98	4.95	10.05	39.52	46.80	52.26	58.72

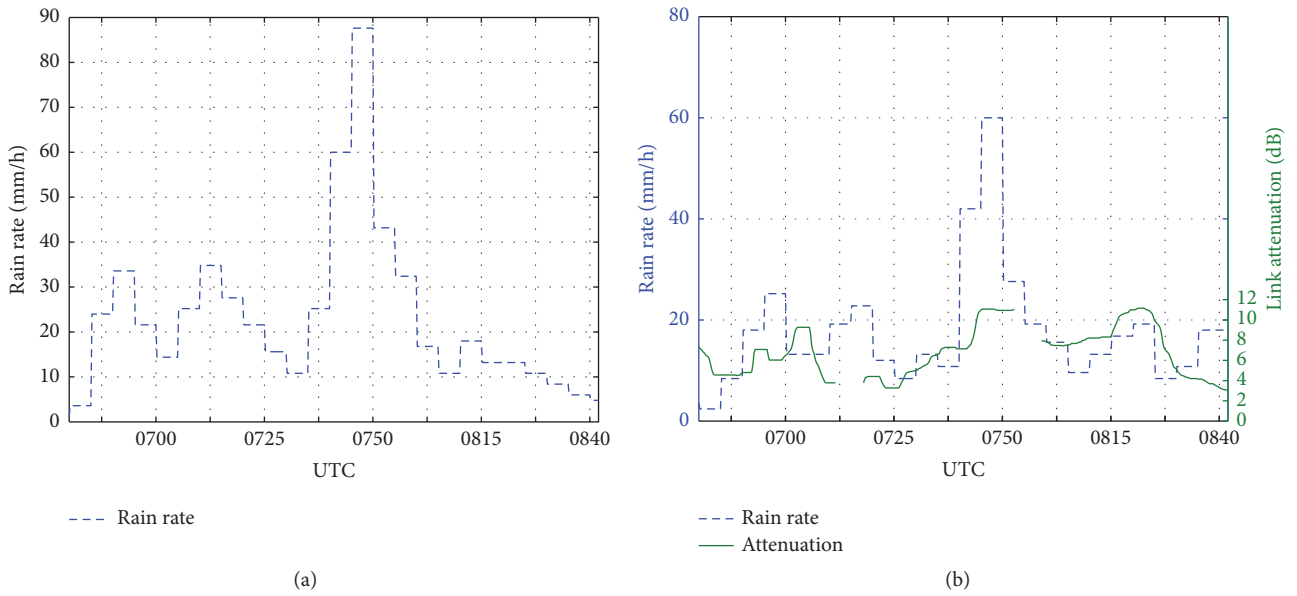

Figure 5: Rain rates measured by (a) gauge 3 and (b) gauge 5 from 0640 to 0842 UTC, 2 June 2015. The link attenuation is also shown in (b).

the precipitation had become a mixed type at that time. The reflectivity was very intense with the maximum value exceeding 55 dBZ due to the extreme heavy rainfall. The instantaneous rain rates during 0640 to 0842 UTC retrieved by gauge 3 and gauge 5 are shown in Figure 5. Since the temporal resolution of rain gauge measurements is 5 min, the instantaneous rain rate I_t (in mm/h) is calculated as $I_t = (G_t - G_{t-1})/5\,\text{min} * 60\,\text{min}$, where G_t is the gauge measurement at current time and G_{t-1} is the gauge measurement at previous recording time. Then all the instantaneous rain rates from $t-1$ to t are set to be I_t.

The rainfall measured by the gauges was very heavy with a maximum rain rate of 88 mm/h in Figure 5(a). The heavy rainfall lasted for a long period at some areas. It was reported that the daily cumulative rainfall amount was the maximum during the prior 10 days of June in Nanjing city since 1961. The path attenuation recorded by ML1 is also plotted in Figure 5(b) together with the rain rate measured by gauge 5 which was located just in the link path (about 4.95 km away from the link transmitter). It can be seen that the heavy rainfall caused strong attenuation (greater than 10 dB) during some periods. Considering that the link path was only 7.5 km, the specific attenuation exceeded 1.33 dB/km at these times. Note that there was an obvious downpour around 0750 UTC when the link attenuation data were missing due to the severe attenuation. The link attenuation at 0720 UTC was also missing but there was no related rainfall peak. The possible reason is that there is a certain mismatch between the point measurement of rain gauge and the path measurement of microwave link, especially for the convective rainfall with rapid spatial and temporal variation.

3.2.2. Data Preprocessing

(a) Clutter Removing. Considering that the microwave link was near the surface, only data in the lowest elevation (1°) of the XR were corrected with the ACML method. Before applying the correction algorithm, it was necessary to remove the ground clutter from radar reflectivity data. The classification of radar clutter was performed using a fuzzy logic classifier proposed by [24]. The features used in the classification include the radial velocity, the texture of the reflectivity, the texture of the differential reflectivity, and the correlation coefficient. The texture of a given point was calculated using the standard deviation of a 3° × 1.275 km (17 data points along radial) window with the point to be classified in the center.

(b) Noise Removing. It was important to remove fluctuations associated with noises in the profiles of radar differential propagation phase φ_{DP}, reflectivity Z_H, and link attenuation. Moving average windows of 17 data points (1.275 km) and 41 data points (3.075 km) were applied to Z_H and φ_{DP} data, respectively. In the case of link attenuation, a moving average window of 8 data points (corresponding to 2 minutes) was adopted.

(c) Attenuation Matching of Radar and Link. Since the frequency of the link (9.47 GHz) differs from that of the XR (9.19 GHz), the attenuation at link frequency must be transferred to that at radar frequency before comparing the mean specific attenuation retrieval results. According to the microwave attenuation model for rain [25], the ratio of attenuation from 9.19 GHz to 9.47 GHz (A9.19/A9.47) versus rain rate is plotted in Figure 6.

It can be seen that the ratio is close to 1 due to the small difference between the two frequencies. The ratio increases with the rainfall rate and the increasing rate becomes lower within a dynamic range of less than 0.03 when rain rate exceeds 10 mm/h. Calculation results also show that temperature and drop shape have very little effect on the ratio (not shown). According to the rain rate distribution in the

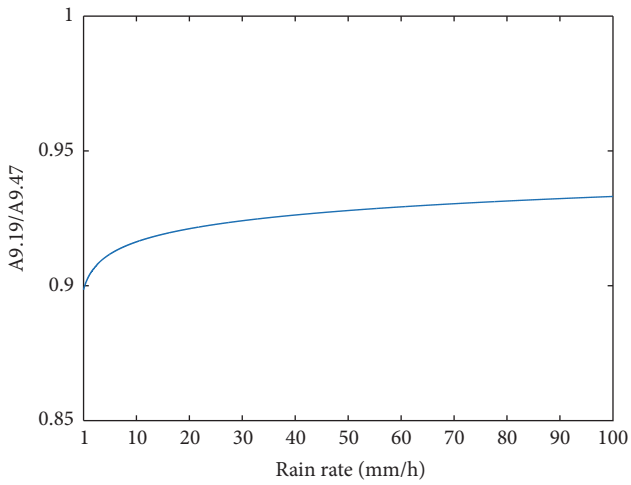

Figure 6: Relationship between specific attenuation due to rain at 9.19 GHz and 9.47 GHz.

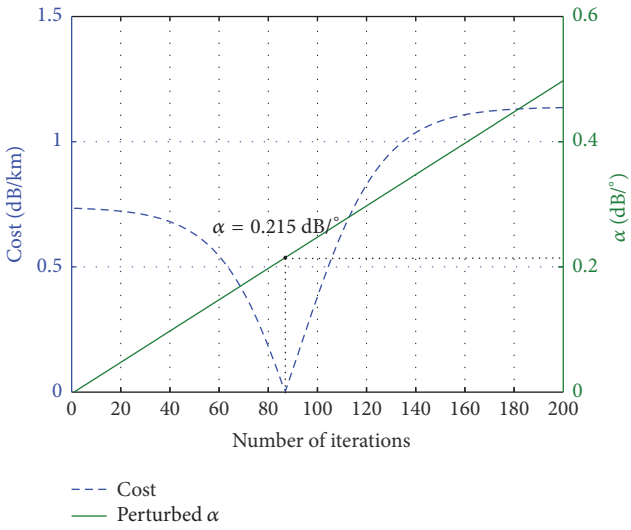

Figure 7: Example of the optimization of α.

experimental cases, the ratio A9.19/A9.47 was set to be 0.912. So, (9) was rewritten to be

$$A_{\mathrm{ML}} = \frac{\mathrm{Attenu}_{\mathrm{ML}} \times 0.912}{L_{\mathrm{ML}}}. \tag{12}$$

3.2.3. Attenuation Correction and QPE Results. The optimal values of correction coefficient α were determined by an iterative procedure in the ACML as shown in Figure 1. An example of α optimization is illustrated in Figure 7.

The variation range of the coefficient α was set from 0.01 to 0.5 dB$(^\circ)^{-1}$ which was a bit larger than the variation range concluded in those previous literatures. As α changed, the cost function defined in (11) fluctuated as shown in Figure 7. The perturbed value of α (0.215 dB$(^\circ)^{-1}$ in Figure 7) corresponding to the minimum was found by golden-section search method. This α was chosen as the optimal coefficient.

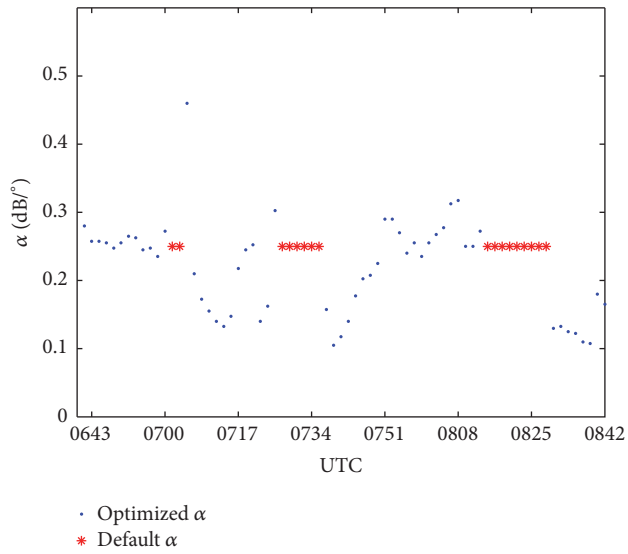

Figure 8: Distribution of the optimized α for the case of 2 June 2015.

The result of the optimized α during the rain event is shown in Figure 8.

During 0640 to 0842 UTC, there were 73 volume scan data collected by the XR. For each reflectivity PPI data of the lowest elevation (1°) in volume scan data, an optimal α was determined using the ACML method. It can be seen from Figure 8 that most of the optimized α were within 0.105 to 0.34 dB$(^\circ)^{-1}$ and only one exception occurred at 0705 UTC when α equals to 0.46 dB$(^\circ)^{-1}$. The distribution of the optimized α was consistent with the variation range of α (i.e., 0.139 to 0.335 dB$(^\circ)^{-1}$) presented in the previous literature [6]. The mean value of the optimized α was 0.227 dB$(^\circ)^{-1}$ with a standard deviation of 0.062 dB$(^\circ)^{-1}$. Note that some values of α were set to be 0.25 dB$(^\circ)^{-1}$ (indicated as red "$*$" in Figure 8) at the corresponding radar observation times when there was no echo detected along the link path, because α could not be optimized with the ACML method under such condition.

Utilizing these optimized α together with (5), (6), and (3), the specific attenuation A_H and the intrinsic reflectivity Z_H were both retrieved. That is, the radar reflectivity within the azimuth range of 228° to 237° which was crossed by the link was corrected for attenuation. An example of attenuation correction of the reflectivity is shown in Figure 9.

The reflectivity distributions of the XR radar before attenuation correction, after ACML attenuation correction, and after SC attenuation correction within azimuth 228° to 237° at 0730 UTC are shown in Figures 9(a), 9(b), and 9(c), respectively. The reflectivity in the same area observed by the SR at 0729 UTC is shown in Figure 9(d). At each point of this area, the corresponding SR reflectivity is extracted from the lowest elevation (0.5°) scan of the SR. Nine-point median filtering was used to make the reflectivity of the SR smoother and easier to compare with XR. It should be noted that the weak echoes at ranges around 20 to 23 km and 38 to 45 km were caused by partial beam blockage error which could be inferred from the analysis on SR volume scan

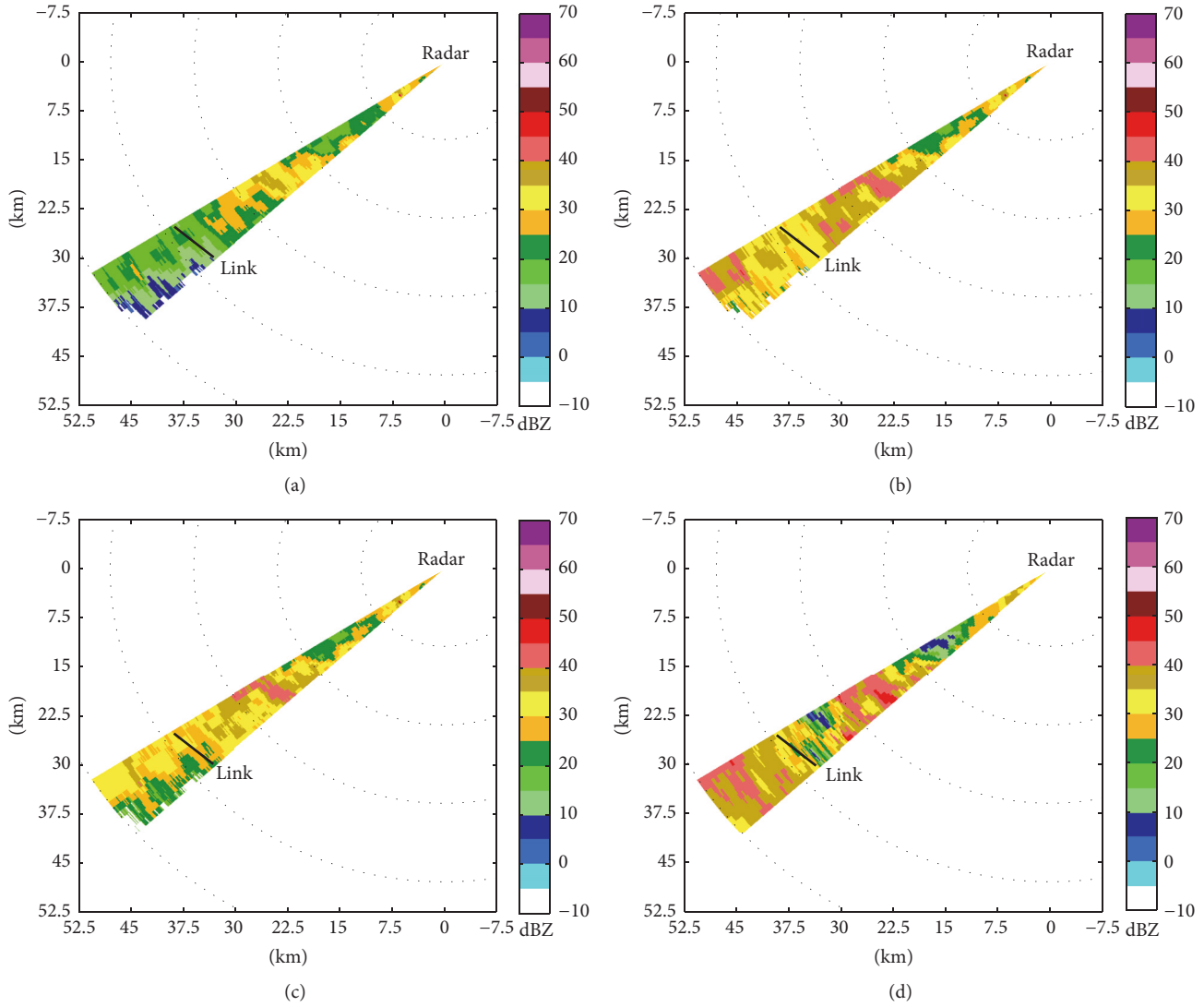

FIGURE 9: Reflectivity of (a) the XR before attenuation correction, (b) the XR after ACML attenuation correction, (c) the XR after SC attenuation correction at 0731 UTC, and (d) the SR at 0730 UTC, 2 June 2015. The microwave link is shown as black straight line in all figures.

data. It can be seen that the reflectivity of the XR before attenuation correction is much lower than that of the SR. The intense echoes detected by SR became weak echoes in XR due to attenuation especially at far ranges (>36 km). After attenuation correction using ACML and SC method, the XR reflectivity was increased obviously and the textures of the echoes changed a lot. The weak echoes on the far side of the XR became more intense. Most of the reflectivity values at far ranges after ACML correction were increased from lower than 20 dBZ to about 30 dBZ. Compared with the result of SC method, the reflectivity after ACML correction was more intense and closer to SR reflectivity.

Figure 10 shows the range profiles of the SR reflectivity and the XR reflectivity before and after correction along the ray of azimuth 236° in Figure 9. It can be seen more clearly that the ACML and SC method both mitigated the errors in XR reflectivity due to attenuation effect. The attenuation

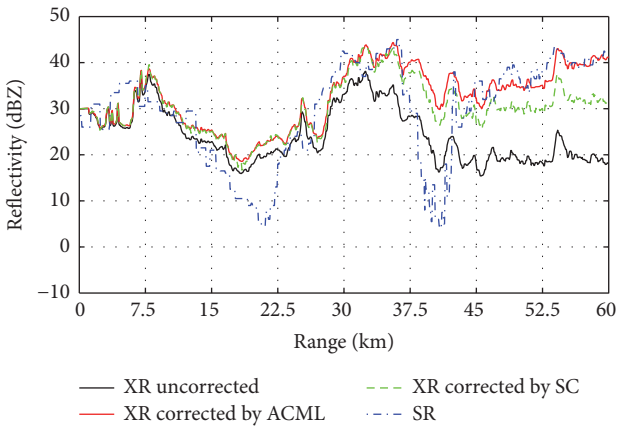

FIGURE 10: The range profiles of SR reflectivity and XR reflectivity before and after correction along the ray of azimuth 236° in Figure 9.

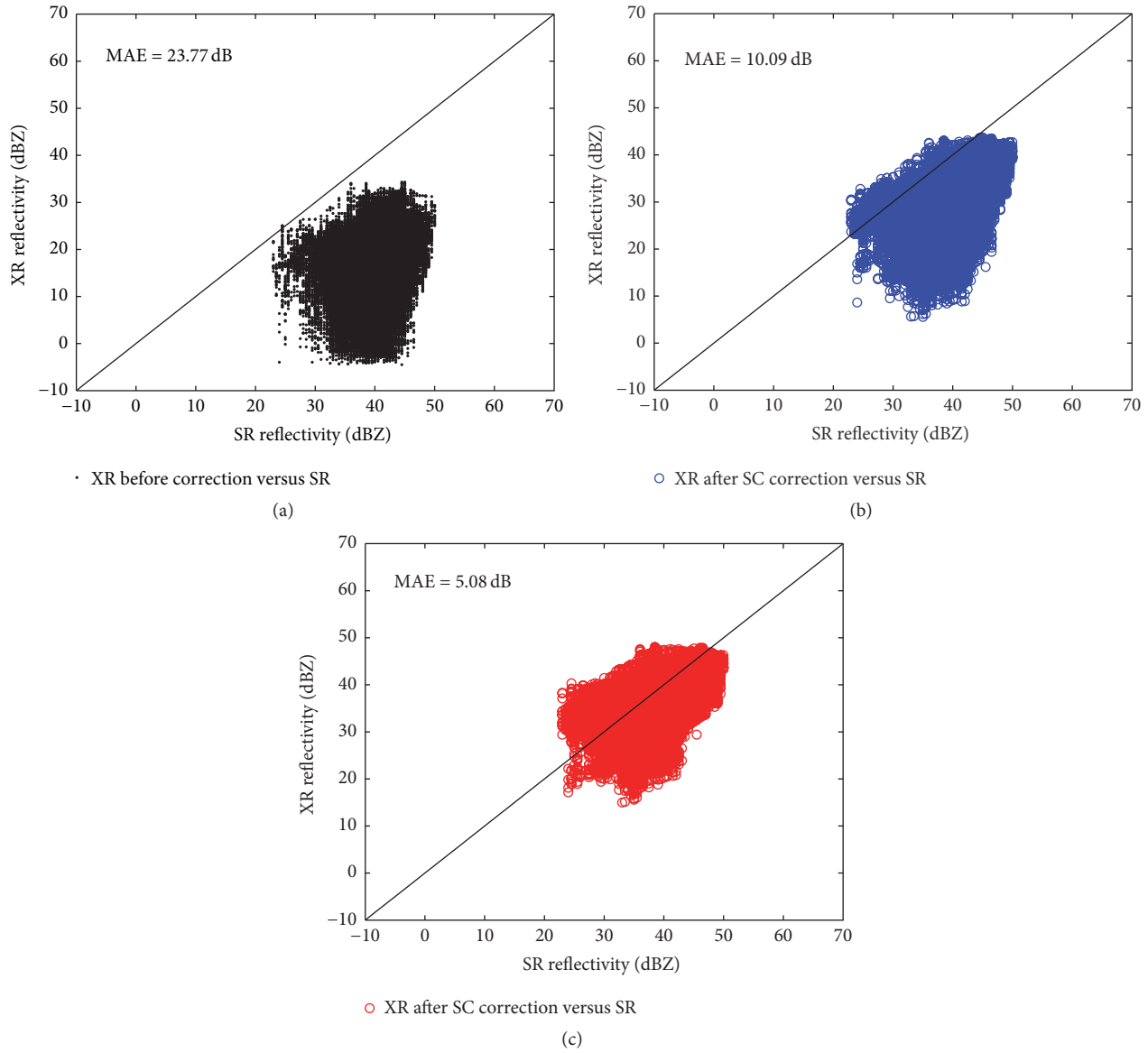

Figure 11: Scatter plot of (a) the XR reflectivity before attenuation correction against the SR reflectivity, (b) the XR reflectivity after SC correction against the SR reflectivity, and (c) the XR reflectivity after ACML correction against the SR reflectivity. All the reflectivities were in the azimuth range from 228° to 237° within the range of 44 and 60 km during 0640 to 0842 UTC. The mean absolute errors (MAEs) are also shown in the figures.

correction amount increased with range. The reflectivity after ACML correction was larger than that after SC correction and more similar to SR especially at far ranges. Note again that the SR was affected by partial beam blockage problem at ranges 20 to 23 km and 38 to 45 km.

To further evaluate the performance of the ACML method, the uncorrected and corrected reflectivities with ACML and SC method against the SR reflectivities were given in Figure 11. Reflectivities in the azimuth range from 228° to 237° and within the range of 44 and 60 km during 0640 to 0842 UTC (101174 points totally) were selected to compare.

It is obvious that the reflectivities corrected with ACML method were more consistent with the SR reflectivity and showed less scatter. The effectiveness of the ACML method was better than the SC method in terms of correction amount.

The impact of attenuation on XR derived rain rate and the effectiveness of the ACML were also evaluated by comparing with rain gauge measurements. Figure 12 shows the comparison of the instantaneous rain rate derived by the uncorrected XR reflectivity, the corrected XR reflectivity, and the measurements of the rain gauge 3.

The rain rates of radar were estimated based on the relationship between radar reflectivity and rain rate (Z-I relationship) using the reflectivity of the XR measurement volumes above the rain gauges. Different Z-I relationships, including $Z = 200I^{1.6}$ for stratiform precipitation and

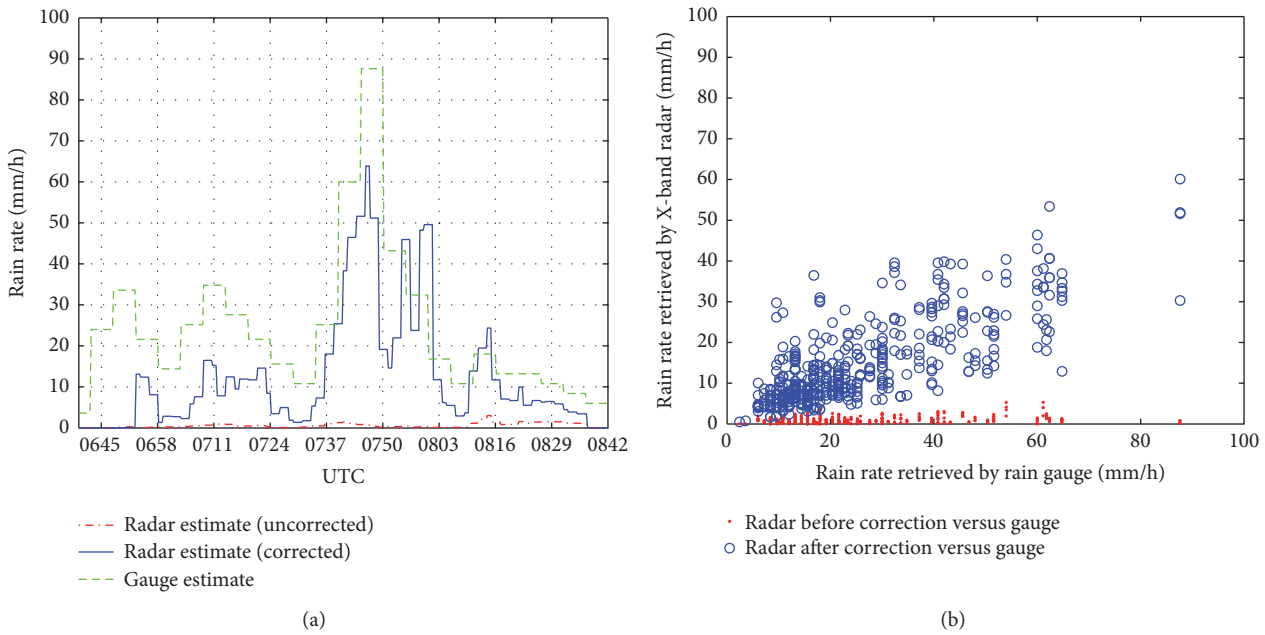

FIGURE 12: (a) Comparisons of rain rates derived by the XR reflectivity before correction, the XR reflectivity corrected with ACML method, and gauge 3 during 0640 to 0842 UTC, 2 June 2015. (b) Scatter plot of rainfall retrieved by the XR against rainfall retrieved by gauges 1 to 6 during the same period as (a).

$Z = 486I^{1.37}$ for convective precipitation, were applied to derive rain rate. Although these Z-I relationships are applicable for different types of precipitations, it is found that the estimation results of rain rate utilizing the two Z-I relationships were very close on the whole. The rain rates retrieved by $Z = 200I^{1.6}$ were a bit larger than those retrieved by $Z = 486I^{1.37}$ and closer to the rain gauge estimations. This indicated again that the precipitation had developed from convective precipitation to stratiform precipitation during the experimental period. As shown in Figure 12(a), the rain rates estimated by the XR before attenuation correction were much lower than that derived by gauge 3 due to the strong attenuation produced by the heavy precipitation. The radar estimated rain rates increased significantly after attenuation correction, and the amplitudes and variations were much closer to the gauge estimations. Figure 12(b) is the scatter plot of all the rain rates retrieved by the 6 gauges against the corresponding (the same location and time) rain rates retrieved by the XR. It can be seen that most radar-derived estimates were less than 5 mm/h, whereas some actual rates approached 90 mm/h. The agreement between the two sets of estimates was significantly improved after the attenuation correction using ACML method. Since the gauges were deployed at different ranges and azimuth directions from the XR, it demonstrated that the ACML worked well in different locations. Although the rainfall was still underestimated overall especially when the rainfall was heavy, the performance of QPE of the XR was obviously improved.

To evaluate the performance of the ACML in a statistical way, the correlation coefficient (CC) between the rain rates of gauges and the X-band radar before and after attenuation correction was calculated, as well as the normalized relative error (RE) which is defined as

$$\mathrm{RE} = \frac{1}{N}\sum_{i=1}^{N}\frac{|I_{Ri} - I_{Gi}|}{I_{Gi}}, \tag{13}$$

where I_{Ri} and I_{Gi} are the rainfall rate estimated by radar and rain gauge, respectively. Term i is the time sampling index and term N is the total number of the sampling times. Table 4 gives the results of RE and CC between the rain rates estimated by gauges and the XR before and after attenuation correction.

From Table 4, it can be seen that the REs were reduced notably. The mean RE of the radar retrieved rain rates decreased from 97% to 53%, which was a significant improvement considering the high rainfall intensity. The correlations between the rain rates obtained by the XR and gauges were also improved obviously after correction. The correlations of the XR-gauge 3 and XR-gauge 4 even changed from negative correlation to strong positive correlation. The mean CC increased from 0.04 to 0.53.

3.3. Analysis of Case II

3.3.1. Precipitation Event. Another rainstorm event occurring on 1 June 2016 was also analyzed to further evaluate the performance of the ACML method. Similar to case I, the precipitation was also developed from a convective precipitation to a mixed type precipitation. Different from case I, the rainfall in this event lasted for a longer time. The ML2 used in this case was different from the ML1 in range to the XR,

Table 4: Relative error (RE) and correlation coefficient (CC) between the rain rates estimated by gauges and the radar before and after attenuation correction.

		Gauge 1		Gauge 2		Gauge 3		Gauge 4		Gauge 5		Gauge 6	
		RE	CC	RE	CC	RE	CC	RE	CC	RE	CC	RE	CC
Radar	Before correction	95.6%	0.234	97.3%	20.1%	98.4%	−0.076	97.4%	−0.069	98.8%	−0.291	96.6%	0.227
	After correction	59.5%	0.317	50.7%	68.5%	50.4%	0.723	54.9%	0.628	51.1%	0.372	52.0%	0.455

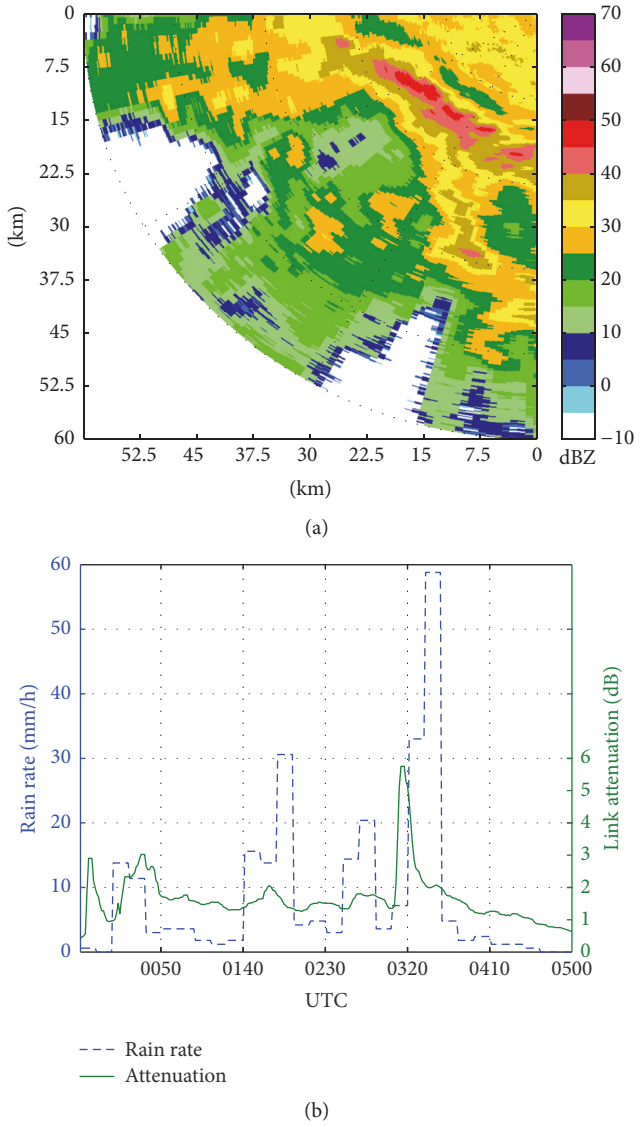

Figure 13: (a) Reflectivity PPI at elevation 1° of the X-band radar at 0330 UTC, 1 June 2016. The circles correspond to radar ranges of 12, 24, 36, 48, and 60 km, respectively. (b) Rain rates derived by gauge 9 from 0000 to 0500 UTC, 1 June 2016. The attenuation recorded by ML2 is also shown in (b).

transmitting frequency and link length. An example of the XR echo and the rainfall derived by gauge 9 (see Figure 3) is shown in Figure 13.

From Figure 13(a), the echoes of the XR at this time were very intense especially at range around 20 km with

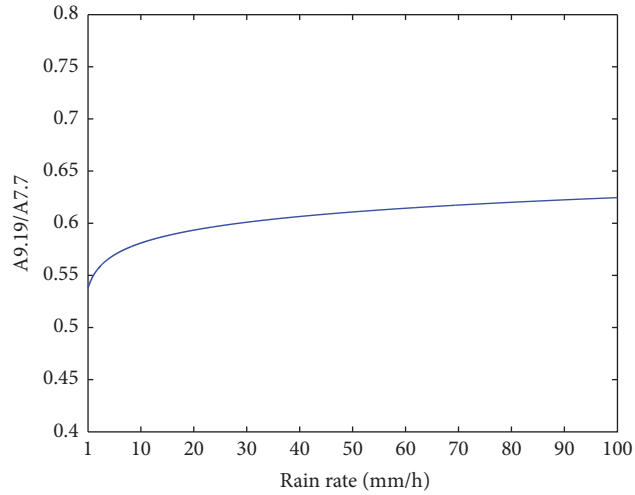

Figure 14: Relationship between specific attenuation due to rain at 9.19 GHz and 7.7 GHz.

maximum reflectivity exceeding 45 dBZ. Because of the strong attenuation caused by the heavy rainfall near the radar, the echoes beyond the intense echoes were very weak. The precipitation far from the XR could not even be detected, leading to the "V" notch echoes at far ranges. The rainfall derived by gauge 9 and the attenuation recorded by ML2 from 0000 to 0500 UTC are both shown in Figure 13(b). It can be seen that although gauge 9 was about 12 km away from the ML2, the time when the attenuation of ML2 and the rain rate of gauge 9 reached their peak values (5.9 dB and 59 mm/h, respectively) was almost the same.

3.3.2. Data Preprocessing. The methods used for clutter removing and noise removing were both the same as in case I. Because the frequency of ML2 (7.7 GHz) differed from that of ML1 (9.47 GHz), it should be studied again on the attenuation matching of the XR and ML2. According to the microwave attenuation model for rain [25], the variation ratio of attenuation from 9.19 GHz to 7.7 GHz (A9.19/A7.7) versus rain rate is plotted in Figure 14.

It can be seen that the ratio varies from 0.54 to 0.625, in which the ratio increases quickly with the rainfall rate and the trend slows when the rain rate exceeds 10 mm/h with a dynamic range of less than 0.05. Setting the ratio adaptively according to the changing of rain rate is helpful to make the retrieval result more accurate. However, in practical applications, rain gauge or other rain measuring instruments may not be available to get rain rate. Therefore, the ratio A9.19/A7.7 was set to be 0.6 considering that the dynamic

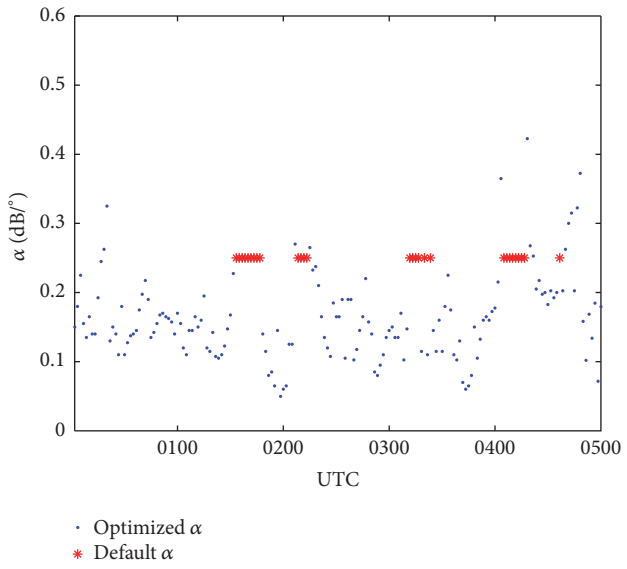

FIGURE 15: Distribution of the optimized α for the case of 1 June 2016.

range of the ratio is very small. Equation (9) was rewritten to be

$$A_{\mathrm{ML}} = \frac{\mathrm{Attenu}_{\mathrm{ML}}/0.6}{L_{\mathrm{ML}}}. \tag{14}$$

3.3.3. Attenuation Correction and QPE Results. The results of the optimized α during this event is shown in Figure 15.

From 0000 to 0500 UTC, there were 180 volume scan data collected by the XR. For each reflectivity PPI data of the lowest elevation (1°) in volume scan data, an optimal α was determined using the ACML method. It can be seen from Figure 15 that most of the optimized α were within 0.05–0.42 $\mathrm{dB}(^\circ)^{-1}$ which was overall consistent with and a bit larger than the variation range of α in literature [6]. The mean value of the optimized α was 0.1749 $\mathrm{dB}(^\circ)^{-1}$ with a standard deviation of 0.0647 $\mathrm{dB}(^\circ)^{-1}$. Note again that some values of α were set to be 0.25 $\mathrm{dB}(^\circ)^{-1}$ at the corresponding radar observation times when there was no echo detected along the link path.

Utilizing these optimized α together with (5), (6), and (3), the radar reflectivity within the azimuth range of 230° to 245° which was crossed by the link was corrected for attenuation. An example of attenuation correction of the reflectivity is shown in Figure 16.

It can be seen from Figure 16 that the reflectivity of the XR before attenuation correction is much weaker than that of the SR. Because of the strong attenuation, precipitations beyond the intense echoes (e.g., precipitation at range about 45 km) were not detected. Even the intense echo at range about 48 km detected by the SR was not detected by the XR. After attenuation correction with ACML and SC method, the XR reflectivity increased obviously. The intense echoes were recovered to a certain extent. Compared with the result of the SC method, the reflectivity corrected with ACML method was more consistent with the SR reflectivity.

It can be seen more clearly from Figure 17 that the proposed method worked well to correct the reflectivity for attenuation. The correction effectiveness was better than the SC method with the correction amount exceeding 25 dB at the end of the ray. The correction result of ACML method was closer to the SR reflectivity. It should be noticed that if the precipitation is not detected by the radar because of strong attenuation, the correction methods cannot recover it.

The rain gauge derived rain rates were utilized again for evaluating the performance of the ACML method in this case. Figure 18 shows the comparison of the instantaneous rain rate derived by the uncorrected XR reflectivity against the corrected XR reflectivity using ACML and SC method.

As done in case I, the rain rates of the XR in Figure 18 were also retrieved by $Z = 200I^{1.6}$. As shown in Figure 18, the agreement between the rainfalls derived by the XR and rain gauges was significantly improved after the attenuation correction using ACML and SC methods. On the whole, the rain rates after ACML correction were larger than those after SC correction and more consistent with the rain rates derived by the rain gauges. It should be noted that the disagreements still existed between the XR and the gauges derived rain rates. Some light rainfalls were overestimated while some heavy rainfalls were underestimated.

Different from case I, the gauges used in case II were farther away from the ML2 (see Figure 3). Gauges 7 and 8 were close to the XR while gauges 9 to 12 were far away from the XR, which demonstrated that the ACML worked well not only in the areas near the ML but also in the areas far from the ML even in such a heavy rainstorm. The performance of QPE of the XR was improved obviously after ACML correction.

3.4. Error Factors Analysis. As shown above, there were still biases between the rain rates estimated by the gauges and the radar after attenuation correction. Firstly, one reason is the spatial mismatch of radar and gauge measurements. Rain gauge measures at a point on the ground while radar makes inference from large volumes at certain heights above gauge. Secondly, factors including radar system bias, radome attenuation, and partial beam blockage can cause errors in radar reflectivity, which will in turn introduce errors into the results of the proposed method. The quality control of the radar data including clutter removal and smoothing of reflectivity and differential propagation phase should be handled carefully. Thirdly, if there is a radar gate along link path without echo, to avoid the problem of beam blocking, the proposed algorithm will not execute. But when radar beam is partially blocked, errors will still be introduced in the estimation of the specific attenuation.

Besides, as described in Section 2, an assumption that the specific attenuation along the link path is equal to the mean specific attenuation derived from the radar measurements above the link path is used in the proposed method. However, the heights of the link path and the radar sampling volumes are different due to the radar elevation and the earth curve. So it is necessary to analyze the impact of the heights difference on the method performance.

As seen from the link, the height of the link path and the central heights of radar beams of elevations 1° and

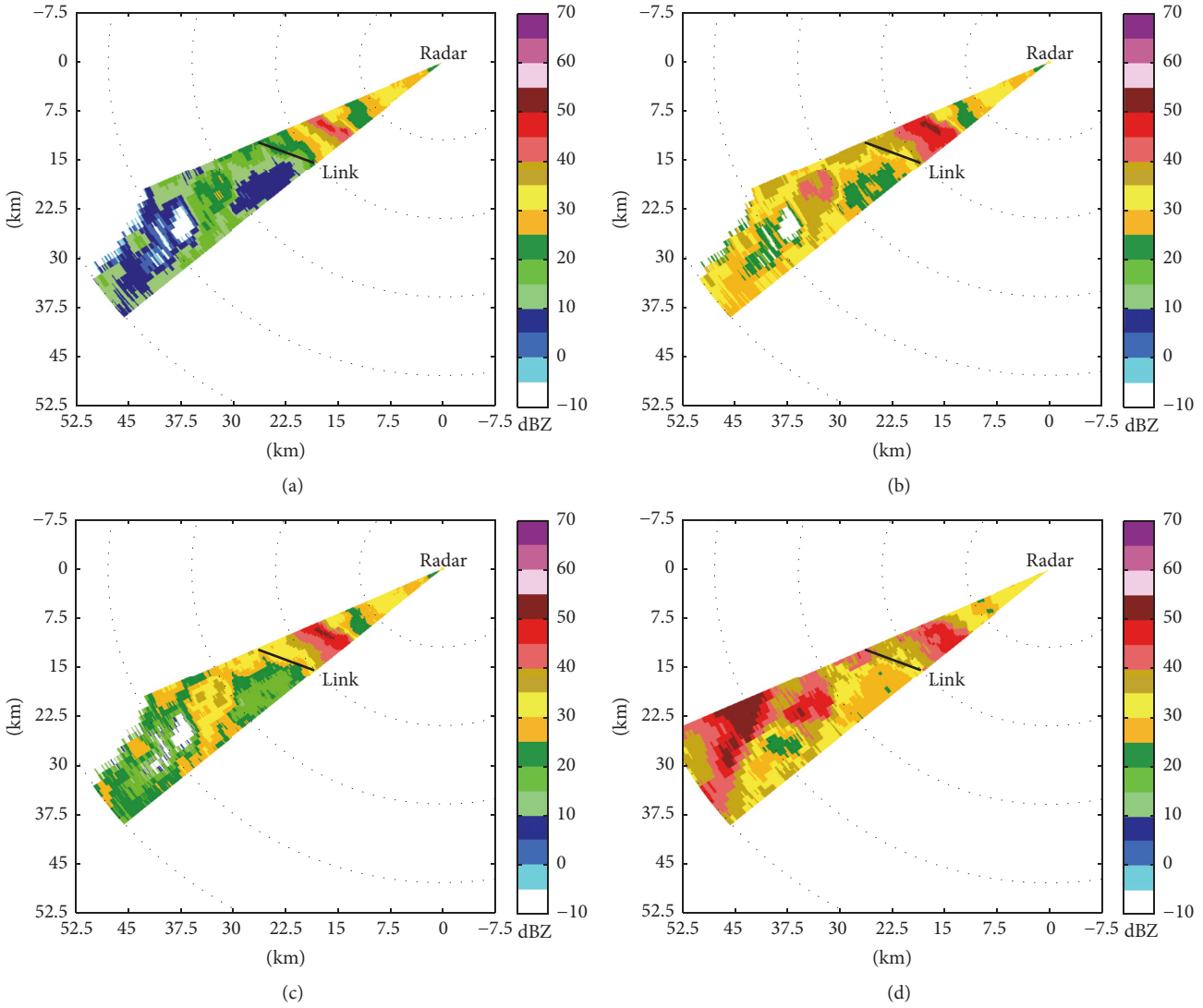

Figure 16: Reflectivity of (a) the XR before attenuation correction, (b) the XR after correction with ACML method, (c) the XR after correction with SC method at 0330 UTC, and (d) the SR at 0330 UTC, 1 June 2016. The microwave link is shown as black straight line in all figures.

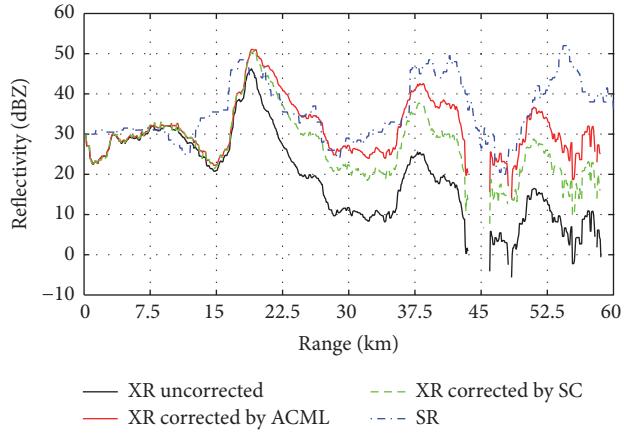

Figure 17: Range profiles of the SR reflectivity and XR reflectivity before and after correction along the ray of azimuth 237° in Figure 16.

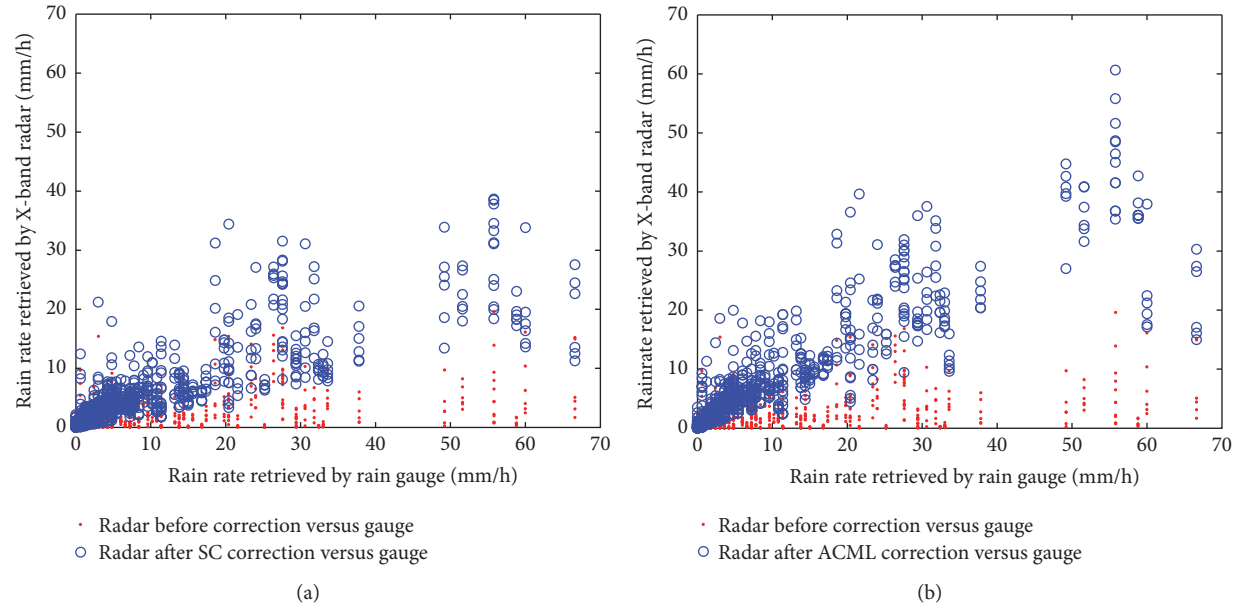

FIGURE 18: Scatter plot of (a) rainfall retrieved by the XR before correction and after SC correction against the rainfall retrieved by gauges 7 to 12 and (b) rainfall retrieved by the XR before correction and after ACML correction against the rainfall retrieved by gauges 7 to 12 during 0000 to 0500 UTC, 1 June 2016.

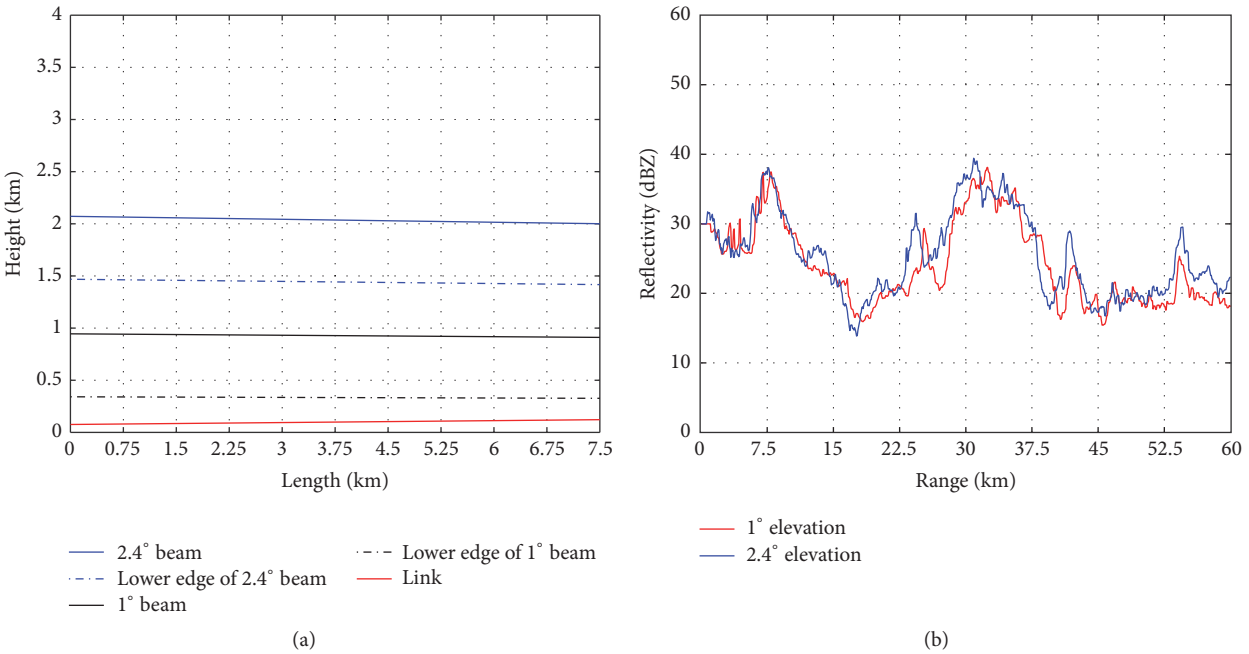

FIGURE 19: Comparisons of (a) heights of the link and radar beams and (b) range profiles of reflectivity of the 1° and 2.4° elevation at azimuth 236° in Figure 9.

2.4° calculated under the standard atmosphere criterion are shown in Figure 19(a), where the heights of the lower edges of the 1° and 2.4° beam are also shown. Figure 19(b) shows the radar reflectivity range profiles of 1° and 2.4° elevations at azimuth 236° in Figure 9. It can be seen that the reflectivities of the two elevations match fairly well even in such a severe rainstorm. Therefore, it can be inferred that the difference between the precipitations on the link path and at 1° radar beam height might not be too large, which in turn indicates that the assumption is reasonable and can work well for the correction of the attenuated reflectivity although it will lead to some errors in the retrieved results. To control this error within an acceptable range, the link used in the proposed method cannot be deployed too far away from the radar

and the elevation of the radar should be as low as possible. The vertical profile of reflectivity (VPR) technique will be investigated and applied in the method to further reduce the error.

Another performance decreasing factor of the ACML is the constant ratio α assumption in the correction area. In fact, α cannot maintain to be a constant due to different temperatures and drop shapes. So the constant α assumption is just a "mean value" solution to the problem and can cause errors in the correction of radar reflectivity, especially in convective rainfall case where the DSDs vary much at different areas. When different microwave links crossing different radar azimuth ranges are available, different optimal α for a particular area can be obtained. Furthermore, when multiple microwave links at different radar ranges are available, the performance of the ACML method can be further improved by applying different optimal α at different ranges.

In addition, the proposed ACML method can only correct the reflectivities within the azimuth range crossed by microwave link. It will be out of work when there is no precipitation above the link path or the attenuation caused by rain is too strong for the radar to detect the returned power. These problems can also be resolved when more links deployed at different ranges and azimuths of the radar are available.

4. Conclusions

A method for attenuation correction of radar reflectivity using synchronous measurements of arbitrary oriented microwave link (ACML) is presented. By minimizing the difference between the mean specific attenuations along the link path retrieved by microwave link and radar, the ratio α of specific attenuation to specific differential phase which is a key parameter in attenuation correction schemes is optimized. The proposed method was applied with real data of an X-band radar and measurements of two microwave links during two rainstorms. The results show that the variation range of the optimized α was overall consistent with that presented in previous studies. The radar reflectivity increased notably after attenuation correction with these optimized α, especially at long distances. Compared with the SC method, the correction amount is larger and the corrected reflectivity is much closer to the reflectivity of a nearby S-band radar. The effectiveness of the method was also evaluated by comparing the rain rates estimated by the radar and those estimated by the rain gauges. The rainfall rates estimated by the X-band radar after correction with ACML method were increased significantly and more consistent with the gauge measurements. The experimental results also show that the proposed ACML method can achieve good performance even in the areas far from the microwave link. In spite of some uncertainties, the ACML method appears to be rather robust.

In addition, compared with previous attenuation correction methods which request microwave link to be radial oriented, the ACML is obviously more effective and more applicable for utilizing arbitrary orientation link. The correction area is also enlarged from one radar ray to the area crossed by the link. More microwave links can be utilized to compensate radar observations and improve the ability for QPE and other quantitative applications. The effectiveness can be further improved by using more links around radar. Since the microwave links have been widespread around the world, the proposed method can be extended in many regions and occasions without any additional costs.

Conflicts of Interest

The authors declare no conflicts of interest.

Authors' Contributions

Peng Zhang, Xichuan Liu, Zhaoming Li, and Kun Song conceived and designed the experiments as well as analyzing the data; Peng Zhang and Zeming Zhou wrote the paper; Pinglv Yang helped perform the statistical analysis.

Acknowledgments

This work was supported by the Open Fund of Jiangsu Key Laboratory of Meteorological Observation and Information Processing (Grant no. KDXS1306), the Jiangsu Province Natural Science Foundation of China (Grant no. BK20150708), and National Natural Science Foundation of China (Grant nos. 41505135, 41475020, and 61473310).

References

[1] H. Chen and V. Chandrasekar, "The quantitative precipitation estimation system for Dallas-Fort Worth (DFW) urban remote sensing network," *Journal of Hydrology*, vol. 531, pp. 259–271, 2015.

[2] W. Hitschfeld and J. Bordan, "Errors inherent in the radar measurement of rainfall at attenuating wavelengths," *Journal of Meteorology*, vol. 11, no. 1, pp. 58–67, 1954.

[3] V. N. Bringi, V. Chandrasekar, and N. Balakrishnan, "An examination of propagation effects in rainfall on radar measurements at microwave frequencies," *Journal of Atmospheric and Oceanic Technology*, vol. 7, no. 6, pp. 829–840, 1990.

[4] J. Testud, E. le Bouar, E. Obligis, and M. Ali-Mehenni, "The rain profiling algorithm applied to polarimetric weather radar," *Journal of Atmospheric and Oceanic Technology*, vol. 17, no. 3, pp. 332–356, 2000.

[5] V. N. Bringi, T. D. Keenan, and V. Chandrasekar, "Correcting C-band radar reflectivity and differential reflectivity data for rain attenuation: a self-consistent method with constraints," *IEEE Transactions on Geoscience and Remote Sensing*, vol. 39, no. 9, pp. 1906–1915, 2001.

[6] S.-G. Park, V. N. Bringi, V. Chandrasekar, M. Maki, and K. Iwanami, "Correction of radar reflectivity and differential reflectivity for rain attenuation at X band. Part I: theoretical and empirical basis," *Journal of Atmospheric and Oceanic Technology*, vol. 22, no. 11, pp. 1621–1632, 2005.

[7] S. Lim and V. Chandrasekar, "A dual-polarization rain profiling algorithm," *IEEE Transactions on Geoscience and Remote Sensing*, vol. 44, no. 4, pp. 1011–1021, 2006.

[8] S. Lim and V. Chandrasekar, "A robust attenuation correction system for reflectivity and differential reflectivity in weather

radars," *IEEE Transactions on Geoscience and Remote Sensing*, vol. 54, no. 3, pp. 1727–1737, 2016.

[9] T. Iguchi and R. Meneghini, "Intercomparison of single-frequency methods for retrieving a vertical rain profile from airborne or spaceborne radar data," *Journal of Atmospheric and Oceanic Technology*, vol. 11, no. 6, pp. 1507–1516, 1994.

[10] M. A. Rico-Ramirez, "Adaptive attenuation correction techniques for C-band polarimetric weather radars," *IEEE Transactions on Geoscience and Remote Sensing*, vol. 50, no. 12, pp. 5061–5071, 2012.

[11] J. Kalogiros, M. N. Anagnostou, E. N. Anagnostou, M. Montopoli, E. Picciotti, and F. S. Marzano, "Evaluation of a new polarimetric algorithm for rain-path attenuation correction of X-band radar observations against disdrometer," *IEEE Transactions on Geoscience and Remote Sensing*, vol. 52, no. 2, pp. 1369–1380, 2014.

[12] O. Sendik and H. Messer, "A New Approach to Precipitation Monitoring: a critical survey of existing technologies and challenges," *IEEE Signal Processing Magazine*, vol. 32, no. 3, pp. 110–122, 2015.

[13] A. Overeem, H. Leijnse, and R. Uijlenhoet, "Retrieval algorithm for rainfall mapping from microwave links in a cellular communication network," *Atmospheric Measurement Techniques Discussions*, vol. 8, no. 8, pp. 8191–8230, 2015.

[14] S. Trömel, M. Ziegert, A. V. Ryzhkov, C. Chwala, and C. Simmer, "Using microwave backhaul links to optimize the performance of algorithms for rainfall estimation and attenuation correction," *Journal of Atmospheric and Oceanic Technology*, vol. 31, no. 8, pp. 1748–1760, 2014.

[15] S. Krämer, H.-R. Verworn, and A. Redder, "Improvement of X-band radar rainfall estimates using a microwave link," *Atmospheric Research*, vol. 77, no. 1–4, pp. 278–299, 2005.

[16] A. R. Rahimi, A. R. Holt, G. J. G. Upton, S. Krämer, A. Redder, and H.-R. Verworn, "Attenuation calibration of an X-band weather radar using a microwave link," *Journal of Atmospheric and Oceanic Technology*, vol. 23, no. 3, pp. 395–405, 2006.

[17] D. S. Zrnić, T. D. Keenan, L. D. Carey, and P. May, "Sensitivity analysis of polarimetric variables at a 5-cm wavelength in rain," *Journal of Applied Meteorology and Climatology*, vol. 39, no. 9, pp. 1514–1526, 2000.

[18] T. D. Keenan, L. D. Carey, D. S. Zrnić, and P. T. May, "Sensitivity of 5-cm wavelength polarimetric radar variables to raindrop axial ratio and drop size distribution," *Journal of Applied Meteorology and Climatology*, vol. 40, no. 3, pp. 526–545, 2001.

[19] G. Delrieu, S. Caoudal, and J. D. Creutin, "Feasibility of using mountain return for the correction of ground-based X-band weather radar data," *Journal of Atmospheric and Oceanic Technology*, vol. 14, no. 3, pp. 368–385, 1997.

[20] L. D. Carey, S. A. Rutledge, D. A. Ahijevych, and T. D. Keenan, "Correcting propagation effects in C-band polarimetric radar observations of tropical convection using differential propagation phase," *Journal of Applied Meteorology and Climatology*, vol. 39, no. 9, pp. 1405–1433, 2000.

[21] A. Zinevich, H. Messer, and P. Alpert, "Prediction of rainfall measurement errors using commercial microwave communication links," *Atmospheric Measurement Techniques Discussions*, vol. 3, no. 3, pp. 2535–2577, 2010.

[22] C. Chwala, A. Gmeiner, W. Qiu et al., "Precipitation observation using microwave backhaul links in the alpine and pre-alpine region of Southern Germany," *Hydrology and Earth System Sciences*, vol. 9, no. 1, pp. 741–776, 2012.

[23] W. H. Press, S. A. Teukolsky, W. T. Vetterling, and B. P. Flannery, *Golden Section Search in One Dimension. Numerical Recipes: The Art of Scientific Computing*, ISBN 978-0-521-88068-8, Cambridge University Press, New York, NY, USA, 3rd edition, 2007.

[24] Y. J. Xiao, B. Wang, X. H. Chen, J. W. Cao, and X. M. Yang, "Differential phase data quality control of mobile X-band dual-polarimetric Doppler weather radar," *Plateau Meteor*, vol. 31, no. 1, pp. 223–230, 2012 (Chinese).

[25] R. ITU-R, Recommendation ITU-R P.838-3 Specific attenuation model for rain for use in prediction methods, 2005.